Multi-port cavity model and low-level RF systems design for VHF gun

Kui Liu[1,2] · Lin Li[3] · Cheng Wang[1,2] · Qiang Gu[3] · Ming-Hua Zhao[1]

Abstract Very high frequency (VHF) photocathode guns have excellent performance and are being increasingly selected as electron sources for high-repetition-rate X-ray free-electron lasers. As a highly loaded quality factor cavity, the VHF gun requires high stability in the amplitude and phase of the cavity field. However, the gun is microwave powered by two solid-state power sources through two separate power couplers. The input difference between the two power couplers will influence the stability of the cavity field. To systematically study this influence and obtain measurement formulae, a multi-port VHF gun LCR circuit model is built and analyzed. During the warm-up condition, the cavity structure will be deformed due to the large-scale change in the cavity temperature. Then, the deformation will result in cavity resonant frequency changes. To prevent the mechanic tuner from suffering damages due to the frequent and long-distance movement for correcting the cavity resonant frequency, a self-excited loop (SEL) control system is considered for changing the loop phase and make the loop frequency follow the resonant frequency. In this study, a steady-state model of the VHF gun cavity is built for obtaining the optimal input coupler coefficient and the stability requirement of the forward voltage. Then, the generator-driven resonator and SEL control system, which combine with the VHF multi-port modeling, are modeled and simulated. The simulated results show that the SEL system can perfectly operate in the process of condition and warm-up.

1 Introduction

The Shanghai high-repetition-rate X-ray free-electron laser and extreme light facility (SHINE) will include the first 8-GeV high-repetition-rate X-ray free-electron laser (XFEL) in China. The XFEL will be operated at 1 MHz repetition rates and will be driven by a 1.3-GHz continuous wave (CW) superconducting linac. The quality of the electron beam, which highly depends on the electron gun, is the most important factor in the performances of the XFEL [1].

Very high frequency (VHF) photocathode electron guns have several advantages, including low radio frequency (RF), CW operation mode, relatively large volume, easy photocathode replacement, high electric field gradient, low dark current [2–4], and are selected for X-ray FEL electron guns, such as the advanced photocathode experiment (APEX) gun in Linac Coherent Light Source II (LCLS-II) [5] and the Deutsches Elektronen Synchrotron (DESY) VHF gun in the European XFEL [6]. VHF electron guns need a very high RF microwave power ($\sim 100\,\text{kW}$) under high average current intensity and CW operation. Considering the power capacity of coaxial waveguides and the

✉ Qiang Gu
  guqiang@sinap.ac.cn

✉ Ming-Hua Zhao
  minghuazhao@sinap.ac.cn

1 Shanghai Institute of Applied Physics, Chinese Academy of Sciences, Shanghai 201800, China

2 University of Chinese Academy of Sciences, Beijing 100049, China

3 Shanghai Advanced Research Institute, Chinese Academy of Sciences, Shanghai 201204, China

influence of dipole fields, the RF microwave power is delivered by two power couplers [7–9].

To generate high-quality electron beams, the acceleration field in the VHF electron gun cavity must be very stable. For example, the APEX gun requires RF amplitude stability of 0.01% (root mean square, RMS) and phase stability of 0.04° (RMS) [5]. However, many random and manufacturing errors result in differences in the microwave parameters between two power couplers. The differences in incident signals and nonlinear noise will result in a difference in the input between two power couplers, leading to an unstable electric field. To explore the influences of these differences and develop measurement formulae for low power and high-power measurements, a multi-port transient LCR circuit model is developed in this study.

In addition to intrinsic errors, there are other extrinsic factors that can influence the cavity field stability. In the process of warm-up, the microwave power increases step by step to avoid interlocking that caused by the RF cavity reflection. During the microwave power increase, if the speed of cooling water is constant, the cavity temperature will rise for power dissipation of cavity walls impedance. The cavity structure will be deformed and result in cavity resonant frequency change [10]. If the mechanical tuner is applied for correcting the resonant frequency, it may be damaged due to frequent and long-distance movements. To solve this problem, Fang [11] developed an auto-tuning system to automatically adjust the mechanical tuner and tune the input RF frequency to the cavity resonance frequency by monitoring the zero phase-slope during field decay in superconducting cavities. He presented the proportion relation between the phase-slope and the detuned frequency. However, the detuned frequency is nonlinear with the cavity temperature change, and it is dozens times larger than the bandwidth of the VHF cavity, so this method is not accurate enough.

The self-excited loop (SEL) system is suitable for solving this problem. The fundamental parts of SEL are a linear filter and phase shifter. In low-level RF control systems (LLRFs), the cavity is a narrowband filter, and it oscillates from loop noise. There are only two conditions to be satisfied: the loop gain must be greater than one, and the loop phase must be an integer multiple of 2π [12]. The SEL algorithm has one distinct advantage over generator-driven resonators (GDRs): the frequency difference between the reference and cavity can be obtained and quickly tuned, even if the cavity has been detuned by many bandwidths [13]. The SEL was first used in an analog version in superconducting accelerator resonators by Delayen in 1978 [14]. Then, a digital SEL (DSEL) was developed and implemented to control superconducting cavities at the TeV–Energy

Superconducting Linear Accelerator project (TESLA) test facility and the Continuous Electron Beam Accelerator Facility (CEBAF) in 2001 and 2002, respectively [15–17]. In principle, the phase of CW machines systems do not need to lock to the reference; the SEL is more suitable for accelerating cavities, which operate in CW mode with a highly loaded quality factor, but it can be used for any resonator cavity.

This paper is broadly divided into three parts. The first part details the derivation of the steady-state and transient state mathematics model of the multi-port cavity. The second part introduces the simulation result of the steady-state model of the VHF gun. The third part presents the layout and modeling of the LLRF control system and the simulation results of the SEL/GDR control system using the Simulink Toolbox in MATLAB.

2 Cavity model

The VHF electron gun is microwave powered by two solid-state power amplifiers through two power couplers. Considering two power coupler ports and one field detector port, the VHF gun cavity model can be built into a three-port model. Figure 1 presents the equivalent parallel LCR circuit of the VHF gun cavity. The solid-state power amplifiers are regarded as voltage sources V_1 and V_2.

$$\begin{cases} V_1(\omega, t) = (V_{1_r}(t) + jV_{1i}(t))e^{j\omega t}, \\ V_2(\omega, t) = (V_{2_r}(t) + jV_{2_i}(t))e^{j\omega t}. \end{cases} \tag{1}$$

where ω is the RF angular frequency; Z_1 and Z_2, which are real values, are the impedances of the two transmission lines; R_P is the load of the field detector, which is also a real value; I_B represents the influence of the electron beam; R_0, L, and C are the resistance, inductance, and capacitance of the VHF cavity; β_1, β_2, and β_P are the coupler coefficients of power couplers 1 and 2 and the field detector coupler, respectively; and N_1, N_2, and N_3 are the equivalent transfer rates of the power couplers 1 and 2 and the field detector coupler, respectively.
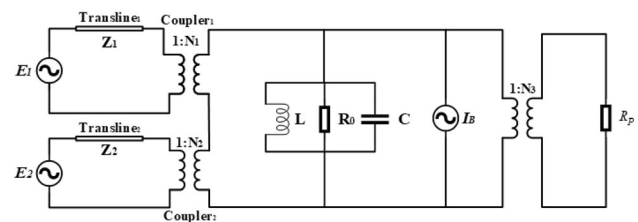

Fig. 1 Equivalent parallel LCR circuit of a three-port model of the VHF gun cavity

$$\begin{cases} N_1 = \sqrt{\dfrac{R_0}{\beta_1 Z_1}} \\[2mm] N_2 = \sqrt{\dfrac{R_0}{\beta_2 Z_2}} \\[2mm] N_3 = \sqrt{\dfrac{R_0}{\beta_P Z_p}} \end{cases} \tag{2}$$

For simplicity, the left parts of the cavity and the field detector coupler are moved to the side of the cavity. Figure 2 shows the equivalent LCR circuit of the VHF cavity at the cavity side. Among the parts, the power sources 1 and 2 are equivalent to current sources I_{G_1} and I_{G_2}.

2.1 Steady-state equation

Schilcher [18] obtained the cavity voltage at the side of the transmission line as follows:

$$\vec{V}'_c = \frac{2Z'_c}{Z'_c + Z_0} \vec{V}_{for}. \tag{3}$$

Here, Z'_c and Z_0 are the impedances of the cavity and transmission line at the side of the transmission line, respectively. Neglecting the influence of beam loading, $\vec{V}_{for} = V_{for_r} + jV_{for_i}$ is the forward voltage on the transmission line.

The cavity field established by the dual-port input can be considered as the superposition of the vector field when each port is input separately. First, assuming that only the power source 1 is operated, the impedance of the VHF cavity at the side of the transmission line 1 is

$$Z'_c = \left(Z_c \| N_2^2 Z_2 \| N_3^2 R_p \right) / N_1^2$$
$$= \frac{\beta_1 Z_1}{1 + \beta_2 + \beta_P + jQ_0\left(\frac{\omega}{\omega_0} - \frac{\omega_0}{\omega}\right)}. \tag{4}$$

Here, $Z_c = R_0 + i\omega L + 1/i\omega C$ is the impedance of the VHF cavity, $\omega_0 = \frac{1}{\sqrt{LC}}$ is the electromagnetic resonant angular frequency, and $Q_0 = \omega_0 R_0 C = \frac{R_0}{L\omega_0}$ is the intrinsic quality factor.
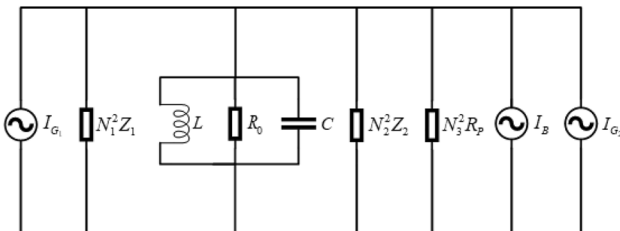

Fig. 2 Equivalent parallel LCR circuit of the VHF cavity at the cavity side

Based on Eq. (3), the cavity voltage $\vec{V}'_{c_1}$ at the side of the transmission line 1 is

$$\vec{V}'_{c_1} = \frac{2Z'_c}{Z'_c + Z_1} \vec{V}_{for_1} = \frac{2\beta_1}{1 + \beta_T + jQ_0\left(\frac{\omega}{\omega_0} - \frac{\omega_0}{\omega}\right)} \vec{V}_{for_1}. \tag{5}$$

Here, $\beta_T = \beta_1 + \beta_2 + \beta_P$, and $\vec{V}_{for_1}$ is the forward voltage on the transmission line 1.

From the measurement equations [19, 20], we obtain the transmitted voltage $\vec{V}_{t_2}$ from power source 1 on the transmission line 2. Because the VHF cavity is a single-cell cavity and the power couplers are both under coupling, the $\vec{V}_{t_2}$ can be inferred when the impedances of the two transmission lines are ($Z_1 = Z_2$).

$$\vec{V}_{t_2} = -\frac{2\beta_1}{1 + \beta_T + jQ_0\left(\frac{\omega}{\omega_0} - \frac{\omega_0}{\omega}\right)} \vec{V}_{for_1} \frac{N_1}{N_2}$$
$$= -\frac{2\sqrt{\beta_1 \beta_2}}{1 + \beta_T + jQ_0\left(\frac{\omega}{\omega_0} - \frac{\omega_0}{\omega}\right)} \vec{V}_{for_1} \tag{6}$$

Similarly, we can obtain the transmitted voltage $\vec{V}_{t_1}$ and the cavity voltage at the side of the other transmission line $\vec{V}'_{c_2}$.

Finally, when both power sources are operated, the cavity voltage at the side of the cavity is

$$\vec{V}_c = N_1 \vec{V}'_{c_1} + N_2 \vec{V}'_{c_2}$$
$$= \frac{2\beta_1 N_1 \vec{V}_{for_1}}{1 + \beta_T + jQ_0\left(\frac{\omega}{\omega_0} - \frac{\omega_0}{\omega}\right)} + \frac{2\beta_2 N_2 \vec{V}_{for_2}}{1 + \beta_T + jQ_0\left(\frac{\omega}{\omega_0} - \frac{\omega_0}{\omega}\right)}. \tag{7}$$

The voltage reflected on the transmission line 1 is

$$\vec{V}_{ref_1} = \vec{V}'_{c_1} - \vec{V}_{for_1} - \vec{V}_{t_1}$$
$$= \frac{2\beta_1 \vec{V}_{for_1} + 2\sqrt{\beta_1 \beta_2} \vec{V}_{for_2}}{1 + \beta_T + jQ_0\left(\frac{\omega}{\omega_0} - \frac{\omega_0}{\omega}\right)} - \vec{V}_{for_1}. \tag{8}$$

The voltage of the field detector is

$$\vec{V}_P = \frac{\vec{V}_c}{N_3} = \frac{2\sqrt{\beta_1 \beta_P} \vec{V}_{for_1} + 2\sqrt{\beta_2 \beta_P} \vec{V}_{for_2}}{1 + \beta_T + jQ_0\left(\frac{\omega}{\omega_0} - \frac{\omega_0}{\omega}\right)}. \tag{9}$$

According to Eq. (8), the phase of the reflected voltage can easily change by 180° due to the tiny change of the forward voltage when β_1, β_2 is equal to 0.5. In the LLRF system, the reflected and forward signals in the ports in the coupler direction can be used to calculate the cavity field, controlled by a feedback loop. Therefore, the frequent change of the phase of the reflected voltage will make the control loop unstable. To avoid this, the coupler coefficient can be set as over coupling. In this study, we set $\beta_1 = 0.51$, $\beta_2 = 0.51$.

2.2 Transient state equation

The baseband cavity transient model is given by [18]

$$\frac{d\tilde{V}_c(t)}{dt} + \left(\omega_{1/2} - j\Delta\omega\right)\tilde{V}_c(t) = R_T\omega_{1/2}\tilde{I}_T(t). \quad (10)$$

Here, $R_T = Z_c\|N_1^2 Z_1\|N_2^2 Z_2\|N_3^2 R_P$; $\Delta\omega = \omega_0 - \omega$. Q_L is the loaded quality factor, and $\omega_{1/2} = \frac{\omega_0}{2Q_L}$ is the half-bandwidth in the cavity frequency domain. $\tilde{V}_c(t) = V_{c_r}(t) + jV_{c_i}(t)$, $\tilde{I}_T(t) = I_{T_r}(t) + jI_{T_i}(t) = \tilde{I}_{G_1}(t) + \tilde{I}_{G_2}(t) + \tilde{I}_B(t)$.

By applying a Laplace Transform to Eq. (10), we obtain a transfer function in baseband:

$$G(s) = \frac{\tilde{V}_c(s)}{\tilde{I}_T(s)} = \frac{\omega_{1/2}R_T}{s + \omega_{1/2} - j\Delta\omega}. \quad (11)$$

Neglecting the effect of the beam loading, the reflected voltage $\tilde{V}_{ref_1}$, $\tilde{V}_{ref_2}$, the detector voltage $\tilde{V}_P$, and the normalized cavity voltage $\tilde{V}_c$ can be written as a matrix (12).

$$\begin{pmatrix}\tilde{V}_{ref_1}\\\tilde{V}_{ref_2}\\\tilde{V}_P\\\tilde{V}_c\end{pmatrix} = \begin{pmatrix}\frac{2\beta_1}{1+\beta_T}\tilde{V}_c(s)-1 & \frac{2\sqrt{\beta_1\beta_2}}{1+\beta_T}\tilde{V}_c(s)\\\frac{2\sqrt{\beta_1\beta_2}}{1+\beta_T}\tilde{V}_c(s) & \frac{2\beta_2}{1+\beta_T}\tilde{V}_c(s)-1\\\frac{2\sqrt{\beta_1\beta_P}}{1+\beta_T}\tilde{V}_c(s) & \frac{2\sqrt{\beta_2\beta_P}}{1+\beta_T}\tilde{V}_c(s)\\\frac{2\beta_1}{1+\beta_T}\tilde{V}_c(s) & \frac{2\beta_2}{1+\beta_T}\tilde{V}_c(s)\end{pmatrix}\begin{pmatrix}\tilde{V}_{for_1}\\\tilde{V}_{for_2}\end{pmatrix}$$

$$(12)$$

3 Cavity simulation

The steady-state model of the VHF gun cavity is built based on Eqs. (7), (8), and (9), and the parameters of the VHF gun cavity are listed in Table 1. To obtain the desired

Table 1 Parameters of the VHF gun cavity

Parameters	Values
$\omega_0/2\pi$ (MHz)	162.5
Q_0	34193
β_1	0.51
β_2	0.51
β_P	1e−4
R_s (MΩ)	7.06
Z_1 (Ω)	50
Z_2 (Ω)	50
$\omega_{1/2}/2\pi$ (kHz)	9.31

high-quality electron beam, the stability of the VHF cavity field is required to be 0.04% (RMS) in amplitude and 0.01° (RMS) in phase. In order to acquire the balanced field distribution, the criterions of the microwave parameter difference and the incident signals difference between two input couplers will be discussed in this section. The influence of the detuned resonant frequency is not discussed in this section.

3.1 Optimal input coupler coefficient

The amplitudes and phases of the two forward voltages are set as constant values: 1 V and 45°, respectively. The simulation results present the amplitude of the reflected voltage 1 increases with increasing β_1, but the relationship between them is nonlinear. This can be explained through Eq. (8). Similarly, the relationship between the amplitude of reflected voltage 2 and β_2 is also nonlinear. In addition, the amplitude of the field detector voltage is the highest under $\beta_1 = \beta_2$. In other words, the amplitude of the cavity voltage is maximum. When the value of $|\beta_1 - 0.51|$ and $|\beta_2 - 0.51|$ are both less than 0.03, $\Delta Am_{V_P}/Am_{V_P} \times 100\% < 0.04\%$, the amplitude requirement of the cavity field voltage can be met. In addition, the phases of the reflected voltage and cavity voltage are not affected by β_1 and β_2 and are always 45°.

3.2 Influence of the forward power difference

The forward power is proportional to the square of the forward voltage amplitude of the power source, so we can change the amplitude of the forward voltage to substitute the change in forward power. The phases of the forward voltages 1 and 2 are always 45°. The coefficients of the two input couplers are both 0.51. Because the coupling coefficient of the VHF cavity is over coupling, the amplitudes of the reflected voltages 1 and 2 are not minimum when the amplitudes of the forward voltages 1 and 2 are equal. The results show that the amplitude of the field detector voltage increase with increasing amplitude of the forward voltage. When $\Delta Am_{for}/Am_{for} \times 100\% < 0.04\%$ (ΔAm_{for} is the sum of the RMS amplitude change value; Am_{for} is the sum of the amplitudes of the two forward voltages, and the amplitude stability of the cavity voltage meets the requirement. The phases of reflected voltage 1, reflected voltage 2, and the field detector voltage are always 45°, no matter how many times the amplitudes of the forward voltages change.

3.3 Influence of the forward phase difference

In a similar way, the amplitudes of the forward voltages 1 and 2 are fixed to 1 V, and the coefficients of the input
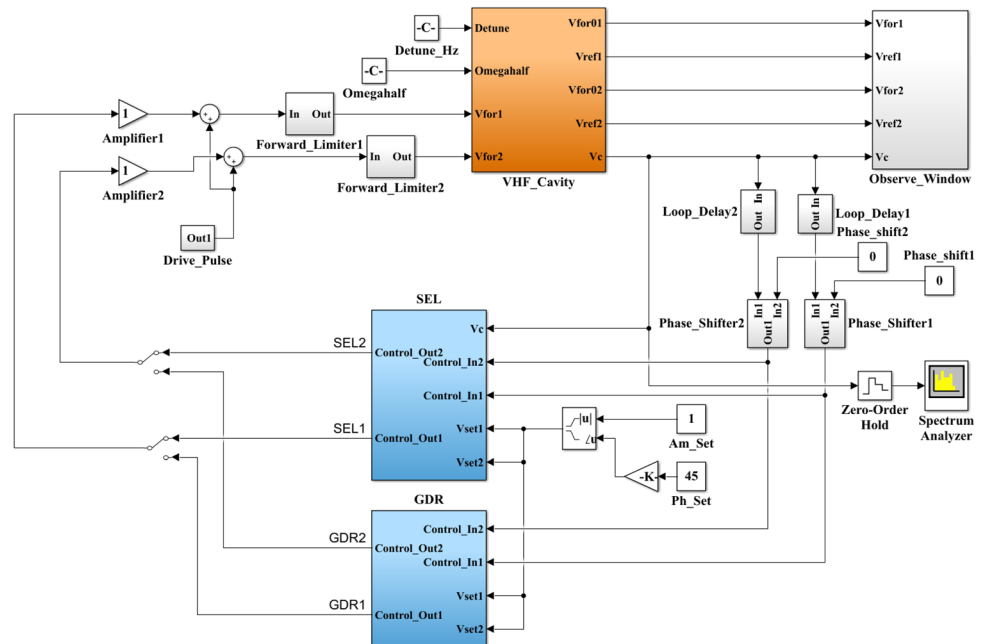
couplers 1 and 2 are both 0.51 in order to explore the field instability due to the differences between the phases of the forward voltages 1 and 2. The simulation results show that the amplitude of the reflected voltage increases with increasing difference between the phases of the forward voltages 1 and 2. When the phases of the forward voltages 1 and 2 are equal, the amplitude of the detector voltage is maximum. In addition, when the difference between the phases of the forward and reference voltages is less than $0.01°$, we can get $\Delta Am_{for}/Am_{for} \times 100\% < 0.04\%$, and the phase stability requirement can be met.

4 Control system simulation

The block diagram from the Simulink modeling for the VHF cavity and LLRF control system is presented in Fig. 3. The block of the VHF cavity is built based on matrix (12) and the parameters in Table 1. The two solid-state amplifiers are separately controlled by two loops to reduce the difference between the two control loops. In order to simulate the time delay of the cable and perform data acquisition and processing, the loop delay block is built, and the delay is set to 0.2 μs. The block of the phase shifter is used to simulate the phase shifter, which is usually used in real control systems. For simplicity, the solid-state amplifier is modeled by a simple amplifier with a gain of 1.

To compare the characteristics of the GDR and SEL modes, the model is first simulated when the resonant frequency is very close to the power source frequency. Then, the SEL mode is also tested after detuning the VHF cavity by many bandwidths.

4.1 Drive signal

To oscillate the control loop, a drive signal is added. This requires the energy of the drive signal to be higher than the quantization noise and much lower than the system state energy. In this study, the drive signal is a single pulse with a 0.5 V amplitude and a 0.1 ms pulse width, which is generated by two-step signals.

4.2 GDR control system

The GDR algorithm is the most popular feedback control method in the LLRF control system. The advantage of GDR is that it can quickly lock the phase when it is used in a pulsed system. The disadvantage is that the cavity resonance frequency must be very close to the power source frequency to prevent the power source from operating in the saturation region. The details of the controller block of the GDR mode are shown in Fig. 4. The reference values of the amplitude and phase are 1 V and 45°, respectively. For correcting the error between set-point values and measured variable values, the proportional–integral–derivative (PID) controller is used in the control system [21, 22]. Because the derivative term is sensitive to the noise signal, the LLRF control system only uses a proportional–integral (PI) controller in a general way [23, 24].

Because the forward and reflected signal of the power coupler 1 are the same as those of the power coupler 2, only the signals of the power coupler 1 are presented in the following discussion. For comparison with the SEL, we assume the detuning frequency is 2 kHz. At steady state, the amplitude and phase stabilities of the cavity field can

Fig. 3 Block diagram of Simulink modeling for VHF cavity and LLRF control system

Fig. 4 Details of GDR
controller block
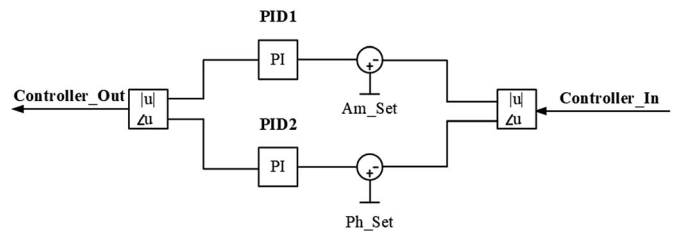
meet the requirements. While the amplitude of the reflected voltage is stable, it is too high, which often causes interlocking, as shown in Fig. 5.

At the initial stage (0–0.3 ms), the amplitude of the forward voltage has a 1.2-V flat peak, which is caused by the forward limiter. The differences between the initial and set-point values of the cavity voltage amplitude result in a high peak on the amplitude of the reflected voltage. Then, the amplitude of the reflected voltage rapidly decreases due to the increasing f cavity voltage. For a similar reason, the phase of the reflected voltage also has a peak at the beginning. Then, it has a 180° change due to the change in the transmission direction. The amplitude and phase of the cavity voltage are quickly locked to 1 V at 0.5 ms, respectively, and have perfect stability in the stable state.

4.3 The SEL control system

Based on the SEL model in the I-Q domain [25] and the SEL amplitude and phase feedback concept [12], the SEL model also includes amplitude and phase feedback, as shown in Fig. 6.
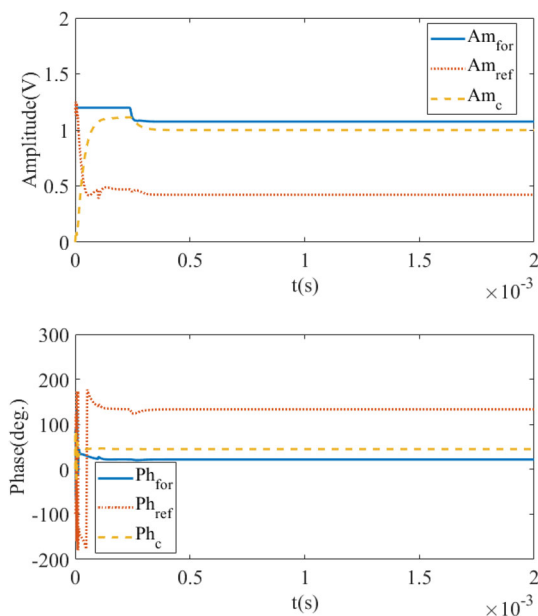

Fig. 5 In GDR mode, the response of the forward, reflected, and cavity field voltages under the resonant frequency detuning is 2 kHz

The yellow part indicates a loop limiter, which guarantees the limit of the loop amplitude and is a fundamental part of SEL. The green part of the model indicates an unlocked SEL, also called a free SEL. During free SEL mode, the loop frequency automatically tracks the resonator frequency, and the amplitude of the cavity field will be stable and unaffected by the cavity detuning. Finally, the light blue part indicates the amplitude feedback loop, which can accurately lock the amplitude at the amplitude reference value.

As shown in Fig. 7, the free SEL mode is turned on at 0 ms; the amplitudes of the forward and reflected voltages are both 0.5 V in the beginning, and then increase due to the loop oscillation. However, the peak is reduced by the forward limiter. The amplitude of the reflected voltage quickly drops as the cavity voltage increases sharply in approximately 1 ms. Then, it becomes relatively low after 0.3 ms. The cavity voltage is stabilized at approximately 1.01 V after 0.3 ms. The phases of the forward, reflected, and cavity voltages all oscillate between −180° and 180°.

At 1 ms, the control mode is switched from free SEL mode to SEL with the amplitude feedback mode. In the initial stage, the difference between the initial phase and set-point value of the cavity voltage results in a small peak in the plot of the amplitude of the forward voltage. Then, the small peak causes a sharp spine of the amplitude of the cavity field and reflected voltages.

As presented in Fig. 8, if the cavity is detuned to 150 kHz, the amplitude of the cavity field can oscillate from the driven signal. However, the gain of the loop must be increased to 2, and a 90° must be added to the phase shifter.

The frequency spectrum of the control loop (Fig. 9) shows that, even if the resonant frequency is detuned by many bandwidths, the loop frequency also follows the resonant frequency and does not affect the peak power of the frequency spectrum in SEL mode.
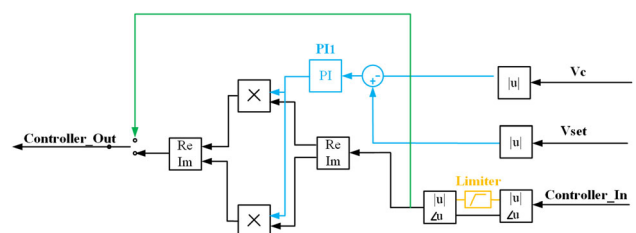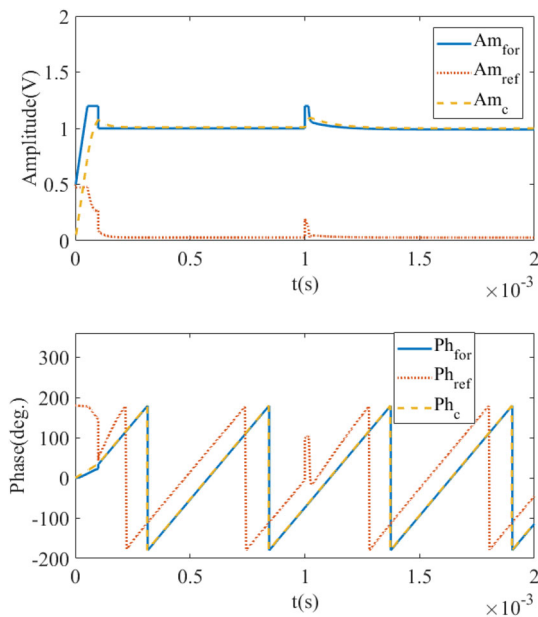

Fig. 6 Details of the SEL controller

Fig. 7 Free SEL (0−1 ms) and SEL modes with amplitude feedback mode (1−2 ms) and the response of the forward, reflected, and the cavity field voltages when the resonant frequency is detuned to 2 kHz
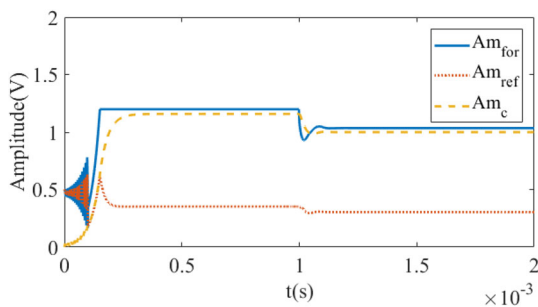
Fig. 8 Response of the forward, reflected, and cavity field voltages in SEL mode with amplitude feedback mode when the resonant frequency is detuned to 150 kHz
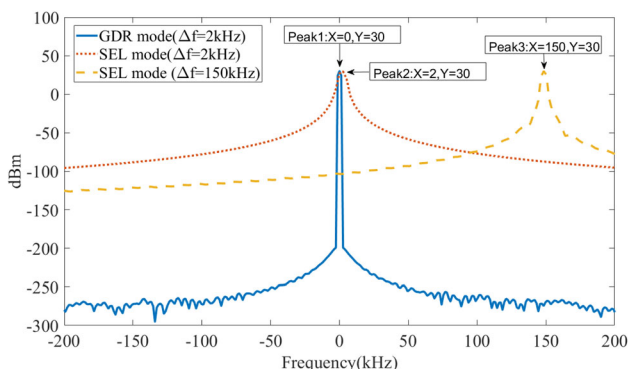
Fig. 9 Frequency spectrum of the GDR and SEL control loops when the cavity is detuned to 2 and 150 kHz

5 Conclusion

A dual-feeding model for VHF gun cavities is developed and modeled in Sects. 2 and 3. Based on the model, the influences of differences in the coupling coefficient, forward power, and forward phase between two couplers are discussed. This helps to evaluate the performance of the VHF cavity in low power and high power modes and satisfy the requirement of the future FPGA firmware.

In Sect. 4, the Simulink models of the GDR/SEL feedback control system for VHF cavities are established and simulated. The results show that the SEL mode has a much smaller reflection than the GDR mode when the resonant frequency is detuned by a few kHz. Furthermore, the SEL mode can follow the resonant frequency and stabilized the amplitude effectively even if the cavity resonant frequency is detuned by many bandwidths. In the future, the GDR/SEL feedback control system will be developed and implemented in the FPGA firmware.

References

1. F. Sannibale, D. Filippetto, C.F. Papadopoulos et al., Advanced photoinjector experiment photogun commissioning results. Phys. Rev. Spec. Top. Accel. Beams **15**, 103501 (2012). https://doi.org/10.1103/PhysRevSTAB.15.103501

2. F. Sannibale, B. Bailey, K. Baptiste et al., Status of the APEX project at LBNL, in *Paper Presented at the 5th International Particle Accelerator Conference* (Dresden, Germany, 2014), pp. 15–20

3. J.F. Schmerge, A. Brachmann, D. Dowell et al., The LCLS-II injector design, in *Paper Presented at the 36th International Free Electron Laser Conference* (Basel, Switzerland, 2014), pp. 25–29

4. R. Huang, D. Filippetto, C.F. Papadopoulos et al., Dark current studies on a normal-conducting high-brightness very-high-frequency electron gun operating in continuous wave mode. Phys. Rev. Spec. Top. Accel. Beams **18**, 013401 (2015). https://doi.org/10.1103/PhysRevSTAB.18.013401

5. G. Huang, K. Campbell, L. Doolittle et al., LCLS-II gun/buncher LLRF system design, in *Paper Presented at the 9th International Particle Accelerator Conference*, (Vancouver, Canada, 29 April–4 May 2018)

6. H.J. Qian, M. Krasilnikov, F. Stephan, A cryocooled normal-conducting and superconducting hybrid CW photoinjector, in *Paper Presented at the 38th International Free Electron Laser Conference* (Santa Fe, USA, 2017), pp. 20–25

7. S. Noguchi, E. Kako, M. Sato et al., KEK ERL cryomodule development, in *Paper Presented at the 50th ICFA Advanced Beam Dynamics Workshop on Energy Recovery Linacs* (New York, USA, 2009), pp. 8–12

8. K. Watanabe, S. Noguchi, E. Kako et al., Development of the superconducting RF 2-cell cavity for the cERL injector at KEK. Nucl. Instrum. Methods A **714**, 67 (2013). https://doi.org/10.1016/j.nima.2013.02.035

9. A. Neumann, M. Abo-Bakr, W. Anders et al., Booster cavity and fundamental power coupler design issues for bERLinPro, in *Paper Presented at the 5th International Particle Accelerator Conference* (Dresden, Germany, 2014), pp. 15–20

10. M.D. Li, Y.B. Zhao, X. Zheng et al., Design and implementation of frequency tracking and amplitude-phase feedback in RFQ low level control system. Nucl. Tech. **41**, 060202 (2018). https://doi.org/10.11889/j.0253-3219.2018.hjs.41.060202. (in Chinese)

11. Z. Fang, T. Kobayashi, Y. Fukui et al., Auto-tuning systems for J-PARC LINAC RF cavities. Nucl. Instrum. Methods A **767**, 135 (2014). https://doi.org/10.1016/j.nima.2014.08.014

12. J. Delayen, in *Self-excited Loop. Jefferson Lab LLRF Workshop*. https://www.jlab.org/intralab/calendar/archive01/LLRF/Delayen.pdf. Accessed 25 April 2001

13. T. Allison, J. Delayen, C. Hovater et al., A digital self excited loop for accelerating cavity field control, in *Paper Presented at the 2007 IEEE Particle Accelerator Conference* (Albuquerque, USA, 2007), pp. 25–29

14. J. Delayen, *Phase and Amplitude Stabilization of Superconducting Resonators*, Ph.D. Thesis, California Institute of Technology (1978)

15. S. Simrock, Achieving phase and amplitude stability in pulsed superconducting cavities, in *Paper Presented at the 2001 Particle Accelerator Conference* (Chicago, USA, 2001), pp. 18–22

16. C. Hovater, P. Chevtsov, J. Delayen, RF system development for the CEBAF energy upgrade, in *Paper Presented at the Proceedings of LINAC 2002* (Gyeongju, Korea, 2002), pp. 19–23

17. C. Hovater, RF control of high Q_L superconducting cavities, in *Paper Presented at the Proceedings of LINAC 2008*, (Victoria, Canada, 29 September–3 October 2008)

18. T. Schilcher, *Vector Sum Control of Pulsed Accelerating Fields in Lorentz Force Detuned Superconducting Cavities*, Ph.D. Thesis, Universitt Hamburg (1998)

19. A. Sun, H.P. Wang, Superconducting RF cavity measurement formulae for an exponential decayed pulse incident power, in *Paper Presented at the 12th International Workshop On RF Superconductivity* (New York, USA, 2005), pp. 10–15

20. L. Chen, S.H. Zhang, M.Y. Li et al., Room-temperature test system for 162.5 MHz high-power couplers. Nucl. Sci. Tech. **30**, 7 (2019). https://doi.org/10.1007/s41365-018-0531-9

21. W.B. Wu, K. Xuan, W. Xu et al., Development of a control system for the fourth-harmonic cavity of the HLS storage ring. Nucl. Sci. Tech. **29**, 153 (2018). https://doi.org/10.1007/s41365-018-0497-7

22. F. Qiu, S. Michizono, T. Miura et al., Real-time cavity simulator-based low-level radio-frequency test bench and applications for accelerators. Phys. Rev. Spec. Top. Accel. Beams **21**, 032003 (2018). https://doi.org/10.1103/PhysRevAccelBeams.21.032003

23. S.S. Sun, J.Q. Zhang, L. Li et al., Linearization of the input and output characteristic curve of a klystron for SXFEL. Nucl. Tech. **40**, 060102 (2017). https://doi.org/10.11889/j.0253-3219.2017.hjs.40.060102. (in Chinese)

24. S. Li, J.Q. Zhang, M. Zhang et al., Implementation of FPGA-based feedforward function in LLRF system for electron LINAC. Nucl. Tech. **39**, 070402 (2016). https://doi.org/10.11889/j.0253-3219.2016.hjs.39.070402. (in Chinese)

25. G. Joshi, P. Singh, V. Agarwal et al., Digital self-excited loop for a superconducting linac. Nucl. Instrum. Methods A **762**, 70 (2014). https://doi.org/10.1016/j.nima.2014.05.115